Articles in PresS. Am J Physiol Lung Cell Mol Physiol (March 18, 2016). doi:10.1152/ajplung.00183.2015

Systematic phenotyping and correlation of biomarkers with lung function and histology in lung fibrosis

Isis E. Fernandez[1], Oana V. Amarie[1], Kathrin Mutze[1], Melanie Königshoff[1], Ali Önder Yildirim[1], Oliver Eickelberg[1]

[1]Comprehensive Pneumology Center, University Hospital of the Ludwig Maximilians University and Helmholtz Zentrum München, Munich, Germany, Member of the German Center for Lung Research.

*Address correspondence to: Oliver Eickelberg, Comprehensive Pneumology Center, Ludwig-Maximilians University Hospital and Helmholtz Zentrum München, Max-Lebsche-Platz 31, 81377 München, Germany, Tel.: 0049(89) 31874666; Fax: 0049(89)31874661; Email: oliver.eickelberg@helmholtz-muenchen.de

Running Title: ICAM1 in pulmonary fibrosis

Funding sources

The study was supported by the Helmholtz Association and the German Center for Lung Research (DZL).

Abstract

To date, phenotyping and disease course prediction in idiopathic pulmonary fibrosis (IPF) primarily relies on lung function measures. Blood biomarkers were recently proposed for diagnostic and outcome prediction in IPF, yet their correlation with lung function and histology remains unclear. Here, we comprehensively assessed biomarkers in liquid biopsies and correlated their abundance with lung function and histology during the onset, progression, and resolution of lung fibrosis, with the aim to more precisely evaluate disease progression in the pre-clinical model of bleomycin-induced pulmonary fibrosis *in vivo*.

Importantly, the strongest correlation of lung function with histological extent of fibrosis was observed at day 14, while lung function was unchanged at day 28 and 56, even when histology showed marked fibrotic lesions. While MMP7, MMP9, and PAI1 were significantly elevated in BAL of fibrotic mice, only sICAM1 was elevated in the peripheral blood of fibrotic mice and strongly correlated with the extent of fibrosis. Importantly, tissue-bound ICAM1 was also elevated in lung homogenates, with prominent staining in hyperplastic type II alveolar epithelial and endothelial cells.

In sum, we show that lung function decline is not a prerequisite for histologically evident fibrosis, particularly during the onset or resolution thereof. Plasma levels of sICAM1 strongly correlate with the extent of lung fibrosis, and may thus be considered for the assessment of intraindividual therapeutic studies in preclinical studies of pulmonary fibrosis.

INTRODUCTION

Repetitive lung injury frequently induces lung fibrosis (13), which leads to impairment of the alveolar-capillary units, enhances fibroblast proliferation and extracellular matrix (ECM) deposition, and aberrant repair processes. These processes ultimately cause irreversible scarring of the lung, often resulting in Idiopathic Pulmonary Fibrosis (IPF)(3, 12). IPF is a rapidly progressive and deadly disease with a median survival of 2-3 years after diagnosis. While two drugs (nintedanib and pirfenidone) have been recently approved for mild-to-moderate IPF in the US and Europe, these slow down the progression, but are unable to reverse or cure IPF (18, 29). To date, the clinical evaluation of IPF most commonly relies on repeated physiologic lung function measurements (e.g. FVC, DL_{CO}) and radiological findings on HRCT, and, when available, histopathology (27). It is currently unclear, however, which of these parameters best correlates with disease progression in IPF (41) (40). Importantly, the survival of patients with interstitial lung disease significantly differs, even when comparing groups with a similar decline in lung function (as assessed by FVC or FEV1) (38), suggesting that the additional use of predictive biomarkers will more accurately project the disease course. As such, defining sensitive parameters that assess and predict the progression of lung fibrosis is imperative, in particular by systematically evaluating recently suggested blood biomarkers in comparison with lung function and histology (5). To begin to address this question, we addressed biomarker profiles in the widely-used bleomycin model of lung fibrosis, in an effort to adequately and precisely correlate biomarkers with physiologic and pathologic parameters (33).

The assessment of drug efficacy in animal models of lung fibrosis has been criticized recently, since several drugs showed efficacy in animal models, but not in clinical studies in IPF. It is important to note, however, that the evaluation of animal models is, in many cases, biased by reader-dependent measurements (23). One particular challenge, e.g., is the interindividual heterogeneity of fibrosis in response to bleomycin, which should be systematically accounted for (22). Furthermore, systemic

evaluation of the bleomycin model is currently limited to biochemical assays, biased selection of fibrosis-affected areas, or reader-dependent scoring of histology sections (e.g. Ashcroft score). Hence, more quantitative assessment of fibrosis or better selection criteria in pre-clinical testing will be critical for drug efficacy evaluation in these models.

Recently, a large prospective biomarker study showed that VCAM1, MMP7, ICAM1, and IL8 are strong predictors of survival in IPF and might thus aid in disease monitoring. Their correlation with lung histology, however, remains unclear (28). Furthermore, a large retrospective IPF cohort study demonstrated that all current available models and commonly measured variables (e.g. FVC, dyspnea score and six-minute walk distance) failed to accurately predict physiological and functional progression of IPF (19). Thus, we sought to assess these biomarkers in several compartments (BALF, peripheral blood) during the initiation, establishment, and resolution of fibrosis, and comprehensively correlated their levels with histology and lung function in order to better define the disease state and severity of lung fibrosis. Finally, we performed serial blood measurements of soluble ICAM1 (sICAM1), the best performing biomarker in our study, and assessed its expression and localization in the lung and primary alveolar epithelial cells during injury and fibrosis.

METHODS

Animals. Pathogen-free female C57BL/6 mice (10–12-weeks old) were obtained from Charles River and maintained at constant temperature and humidity with a 12 h light cycle. Animals were allowed food and water ad libitum. All animal experiments were conducted under strict governmental and international guidelines and were approved by the local government for the administrative region of Upper Bavaria (TVA 55.2-1-54-2532-21-12), as previously described (17).

Induction and assessment of pulmonary fibrosis. Pulmonary fibrosis was initiated by a single intratracheal instillation of 50 µl bleomycin (3U/kg, Sigma Aldrich, Taufkirchen, Germany), dissolved in sterile PBS, and applied using the MicroSprayer Aerosolizer, Model IA-1C (Penn-Century, Wyndmoor, PA). Control mice were instilled with 50 µl PBS. After 7, 14, 28, or 56 days after bleomycin or PBS instillation, lung function was measured using the FlexiVent system (Sireq) and mice were sacrificed for biochemical and histological analysis. BAL (bronchoalveolar lavage) was performed by instilling the lungs with 3×0.5 ml aliquots of sterile PBS to obtain BAL fluid for biomarker analysis, and total/differential cell counts for inflammatory cell recruitment of neutrophils, macrophages, or lymphocytes were measured. Lung tissue was either snap-frozen in liquid nitrogen to determine tissue mRNA/protein expression or fixed by intratracheal instillation of 4% PFA (paraformaldehyde) and embedded into paraffin for staining.

Image acquisition, processing and analysis. At least 3 sections from the same lung were cut and arranged on the same paraffin block, and the slides stained with hematoxilin-eosin (H&E). Stained sections were automatically scanned with a digital Mirax slide scanner system (3DHISTECH, Budapest, Hungary) equipped with a 20× objective with a numerical aperture of 0.75. The actual scan resolution (effective pixel size in the sample plane) at 20× was 0.23 µm. The accompanying software allowed the user to navigate through the captured Whole Slide Image (Zeiss, Germany).

Quantification of fibrosis using semi-automated image analysis. A minimum of 3 whole-lobe cuts of 500 µm from identical mice were exported in high quality tiff files (8). All images were analyzed using an already developed macro (15), which required ImageJ v1.38 or higher. This ImageJ macro was written to quantify the percentage of fibrosis compared with the total amount of tissue within an image. This percentage was determined by quantifying the total tissue areas occupied by dense parenchyma. The threshold was set arbitrarily after the black and white conversion to +/- 5 (205) for all slides. To do so, we converted the image from color to 8-bit, followed by the delimitation of the area of interest (whole

lobe selection) and measurement of the selected area (Figure 2A) as density percentage. The alveolar space was determined by "parenchymal-free" area quantification, which included bronchi and vessels (Figure 2B). We then quantified at least 3 sections (2mm approx. distant from each other in a transversal cut) from each lung; this value was averaged and assigned as the percentage of alveolar space of each individual.

Luminex multiplex assay and ELISA. A multiplex biometric ELISA-based immunoassay was performed using plasma or BALF from PBS- or bleomycin-treated mice, according to the manufacturer's protocols. We used the Mouse Cardiovascular Disease (CDV) panel 1 commercially-available multiplex kit from Millipore (Billerica, MA). MMP-7 and sICAM1 ELISAs were performed using plasma, BALF, or ATII supernatants from PBS- or bleomycin-treated mice, according to manufacturer's protocol (Uscn Life Science Inc. Wuhan, China; Thermo Scientific, Rockford USA, respectively).

Immunofluorescent stainings. Lung tissue was embedded in paraffin and Immunofluorescence analysis was performed as previously described (37). Briefly, sections were stained with anti-mouse ICAM1 (Thermo Fisher Scientific) or E-cadherin (Millipore) overnight at 4°C, washed three times with PBS, and subsequently incubated with the secondary antibodies (1:250 dilutions of Alexa Fluor 568 goat anti-rabbit or Alexa Fluor 488 goat anti-mouse) and DAPI (4',6-diamidino-2-phenylindole, Sigma-Aldrich, St Louis, MO, USA, 1:2000) for 1 hour at room temperature. Finally, the sections were washed three times with PBS and mounted in fluorescent mounting medium (Dako). Images were acquired with an LSM 710 (Zeiss) operated in multitrack mode.

RNA Isolation and Real-Time Quantitative Reverse-Transcriptase PCR (qRT-PCR) Analysis. RNA extraction from mouse tissue was performed using the Roti Quick Kit (Carl Roth, Karlsruhe, Germany), followed by RNA purification with the peqGold RNA isolation kit (Peqlab, Erlangen, Germany), according

to manufacturers' instructions. Quantitative real-time PCR (qRT-PCR) was performed using SYBR Green PCR master mix (Roche Applied Science, Mannheim, Germany).

Immunoblotting. Pulverized mouse tissue was homogenized in Radio-Immunoprecipitation Assay (RIPA) buffer, containing a protease and phosphatase inhibitor cocktail (Roche). Protein concentrations were determined using the Pierce BCA Protein Assay (Thermo Fisher Scientific). Samples were denatured in Laemmli buffer, resolved by SDS-PAGE, and transferred to polyvinylidene diflouride (PVDF) membranes. Nonspecific membrane binding was blocked with 5% low-fat milk in TBS-T (0.1% Tween 20, TBS). Membranes were incubated with the primary antibodies to ICAM1 (Thermo Fisher Scientific) or β-actin (Sigma Aldrich) overnight at 4°C. After washing with TBS-T, the membranes were incubated with secondary antibodies for 1 h at room temperature. Blots were rinsed with TBS-T and visualized with the enhanced chemiluminescence (ECL) system (Thermo Fisher Scientific, Waltham, MA, USA), followed by analysis using the ChemiDocXRS+ imaging system (Bio-Rad, Munich, Germany). Band quantification was performed using ImageJ software (version v1.38).

Primary murine ATII cell isolation and culture. Primary murine ATII (pmATII) cell isolation from PBS- or bleomycin-treated mice was performed as previously described (24). Supernatants were collected, snap-frozen, and 1:2 diluted supernatants were used for the assessment of sICAM1 levels by ELISA.

Statistical Analysis. Results are presented as means ± SD and were considered statistically significant with p-value <0.05. Data of selected groups were compared using one-way ANOVA, followed by the Dunnet *post hoc* test. The Pearson's correlation coefficient (r-value) was used to determine the degree of association between variables and interpreted using Dancey and Reidy's categorization (9). Here, r-values of ±1, ±0.7 to ±0.99, ±0.4 to ±0.69, ±0.1 to ±0.39, and 0 were interpreted as perfect, strong, moderate, weak, or no correlation, respectively. The statistical significance of the correlations was

assessed by p-value. A linear regression analysis between two variables was performed and the best fit curve drawn from data points.

RESULTS

The dynamics of lung injury, fibrosis, and resolution in bleomycin injury

We first sought to perform an extensive phenotypic characterization of the bleomycin-induced fibrosis model over an extended time period up to 56 days after intratracheal application of bleomycin. Lymphocyte and neutrophil cell numbers significantly increased in BALF during the first seven days after bleomycin injury and returned to baseline levels after 28 days. BALF macrophage numbers, in contrast, were significantly increased at all-time points (day 7 to 56) and peaked 14 days after bleomycin injury (Figure 1A). Static lung compliance, a surrogate of tissue stiffness, was significantly decreased 7 days post-bleomycin with a major decrease 14 days after bleomycin instillation. Static compliance returned to baseline levels at day 28 and was significantly increased at day 56 (Figure 1B). Similar observations were made for tissue elastance (Figure 1B). Histologic analysis revealed a peak of lung fibrosis at day 14 after injury, which regressed, but did not completely resolve, by day 56 (Figure 2A).

To avoid reader-dependent bias, we designed a semi-automatized algorithm to calculate the percentage of alveolar space (Figure 2B). After measuring 39 individual mice, including 29 bleomycin-injured mice (n = 8, 9, 5, and 7 for day 7, 14, 28, and 56 after bleomycin application, respectively) and 10 controls (harvested from all time points, for a total of 149 images), we observed a significant drop in alveolar space at day 7 compared with controls. The percentage of alveolar space remained reduced over the entire observation period of 56 days (Figure 2C). We then assessed the correlation strength of % alveolar space with lung function parameters (compliance) using all samples at all-time points. We observed a moderate positive correlation (r = 0.4) for all samples analyzed (Figure 3A). When single time

point correlations were performed, we observed the strongest correlation at day 14 post-treatment, followed by day 7 (Figure 3B). No significant correlations were obtained at day 28 and 56. This indicated that lung function parameters fully recovered to normal values even in the clear presence of histological evidence of fibrosis.

To substantiate these observations, we measured transcript levels of established markers of fibrosis (*col1a1, fn1, loxl2, and tnc*) in lung homogenates over the entire time course. We observed a significant increase in all fibrosis markers during the peak of lung fibrosis (day 14) compared with controls (Figure 4), albeit with different expression dynamics over the entire time course of lung fibrosis. In fact, *col1a1* was exclusively up-regulated at day 14 post treatment, whereas *fn1* was significantly up-regulated from day 14 until day 28. Expression of the ECM-modifying enzyme *loxl2* was increased from day 7 to day 28, and decreased back to basal levels at day 56. Expression of *tnc* was highly increased at day 7, which was maintained up to day 56. These dynamics thus suggest different contributions of these ECM components to injury and scar formation in the lung.

Compartmentalized biomarker signatures during lung injury, fibrosis and resolution

Next, we assessed protein expression using a five-analyte panel containing MMP9, PAI1, E-selectin, VCAM1, and sICAM1, according to previously reported biomarkers in IPF. In addition, MMP7 was measured via ELISA (Figure 5A). Two out of these six candidate proteins were significantly regulated during the onset and resolution of fibrosis when measured by Luminex in plasma: E-selectin was significantly increased at day 7, and significantly decreased at day 56 compared with controls, whereas sICAM1 was significantly increased from day 7 through 28, after which levels normalized again. The increase in circulating sICAM1 was validated by ELISA, which showed a significant increase in sICAM1 levels at day 14 post-bleomycin treatment (Figure 5C). Both assays showed similar regulation of sICAM1,

198 but ELISA values are well-known to underestimate real concentrations compared with Luminex
199 platforms (7). Interestingly, some of these candidate proteins were not detectable in BALF in the same
200 individuals (Figure 5B). From the 6 candidate proteins tested, 4 were detectable in BALF (MMP7, MMP9,
201 sICAM1, and PAI1), out which 2 were significantly increased during fibrosis: PAI1 was significantly
202 increased exclusively at day 7, whereas MMP7 was significantly increased at day 7 and 14, during the
203 peak of fibrosis.

204 We correlated the selected protein levels with pulmonary compliance and analyzed the correlation
205 coefficient of these 2 variables within all measured samples. No significant correlation was observed for
206 MMP9, and VCAM1. A weak but significant correlation was observed for MMP7, and E-selectin; and a
207 stronger and highly significant correlation ($p<0.0001$) for PAI1 and sICAM1 with respect to protein
208 plasma levels and lung function (Figure 6).

209

210 **Compartmentalized regulation of ICAM1 during lung injury and fibrosis**

211 To further determine whether sICAM1 blood levels were regulated during the onset and progression of
212 fibrosis in an intraindividual manner, we performed sequential bleedings from day 0 to day 15 and
213 measured sICAM1 levels every 3rd day, in control and bleomycin-treated mice. We observed that sICAM1
214 levels were significantly increased as fibrosis developed (Figure 7A). Importantly, Western blotting of
215 whole lung homogenates revealed that ICAM1 protein expression levels were significantly increased at
216 day 14, compared with PBS controls (Figure 7B). Immunohistochemical staining demonstrated that
217 ICAM1 was strongly expressed in alveolar epithelial cells and endothelial cells in the healthy lung, while
218 it was prominently expressed in hyperplastic alveolar epithelial cells and endothelial cells during fibrosis
219 (Figure 7D). To confirm this, we investigated whether sICAM1 is shed from alveolar epithelial cells during
220 fibrosis by analyzing supernatants of primary alveolar epithelial (pmATII) cells from PBS- and bleomycin-

221 treated mice (day 14). We observed that supernatants from bleomycin-treated pmATII cells exhibited
222 significantly increased levels of sICAM1, compared with PBS-treated pmATII cells (Figure 7C).

223

224 **DISCUSSION**

225 We have witnessed an unprecedented gain in our understanding of the pathomechanisms driving lung
226 fibrosis in the past years, including the assessment of mRNA and miRNA expression patterns in the
227 fibrotic lung, both in murine and human studies. Two therapies for IPF have recently been approved in
228 Europe, the US, and a variety of other countries (18, 29), both of which decelerate the lung function
229 decline in IPF patients. Despite these major achievements, we are still unable to stop progression, or
230 better reverse the loss of functional lung tissue in IPF (10). The development of better diagnostic tools
231 and continued efforts for drug development in IPF, using better refined and defined animal models and
232 complex phenotypic assays therefore continue to be a major challenge to the scientific community (42).
233 To this end, we sought to comprehensively assess recently described biomarkers in IPF in the bleomycin-
234 induced model of lung fibrosis, in a compartmentalized manner, to increase the accuracy of
235 interventions and outcome measures during drug testing.

236 Although the comparison between the bleomycin-induced model of pulmonary fibrosis and IPF has been
237 highly controversial (2), recent studies show strong commonalities on distinct levels, encouraging the
238 continuous use of the model for preclinical testing (4, 26). In humans, IPF lesions are continuous and
239 progressive, contributing to permanent and irreversible lung scarring. In mice, the bleomycin-induced
240 fibrotic lesions are heterogeneous, time-limited and self-resolving, bringing the advantage of analyzing
241 the dynamics of injury-fibrosis-resolution and assess heterogeneity in an intraindividual manner. At first,
242 the inflammatory phase takes place within the first 7 days, followed by increased ECM deposition with a
243 maximum at day 14, and resolution from day 21-28 onward. Largely, lung function returns to basal
244 levels at 56 days post bleomycin treatment, as we have previously reported (31).

Importantly, the spatio-temporal heterogeneity of lung fibrosis increases the complexity in achieving these goals. Well-established systematic measurements, such as pulmonary function tests (e.g. FVC, FEV_1) are in daily clinical use assessing restrictive lung disease, but they remain unspecific and with limited sensitivity, possibly preventing early detection of patients with lung fibrosis (32). In addition, only 14% of early ILD patients exhibit changes in HRCT (14, 40), whereas 32% of these patients exhibit changes in trans-bronchial biopsy (8). These data strongly suggest that a number of fibrotic lesions, in particular early lesions, are not detected using a combination of up-to-date imaging and lung function measurements in the clinical setting. This notion is supported by the data reported in our study. We show that in mice, the maximum lung function decline was observed at day 14 post-treatment. Lung function returned to baseline levels, whereas histological analysis still demonstrated a significant amount of fibrosis in these individuals, demonstrating the need for specific biomarkers detecting the presence of tissue fibrosis.

To avoid reader-dependent and region-of-interest selection bias, we developed a whole-lung, semi-automatized quantification system. With this method, we were able to provide a robust broader assessment of the affected lung by quantifying the alveolar space loss during fibrosis. In some severe cases, alveolar loss went up to 30%, and was maintained over time, although lung function improved. This might reflect a different molecular/cellular composition of the lung parenchyma during the scar formation process. It is important to clarify that both parameters, lung function and histology, are equally required to understand a given disease process, since each of them may reflect different aspects of the disease. In the lung fibrosis model of adenovirus-mediated overexpression of active TGF-β (6), good correlations between histomorphological, radiological, and functional changes were observed (1). Notably, this model is a progressive and persistent model of fibrosis, supporting that during the peak of fibrosis, but not necessarily during the initiation or resolution thereof, these parameters comprehensively assess the disease status of the individual.

Interestingly, we found that single ECM components vary significantly during the evolution of fibrosis in the lung. For instance, *col1a1* and *fn1* were predominantly increased at the peak of fibrosis (when the lung exhibits maximum stiffness), while other ECM components maintained high expression levels at all time points, supporting that some ECM members might be causally responsible for lung function decline, and therefore critically determine the increased parenchymal stiffness of the lung.

Since physiologic measures and histopathology are at times poor predictors of short- and long-term outcome, we profiled peripheral blood components as reflectors of the fibrotic process. Richards and colleagues recently demonstrated that IPF patients display a unique plasma signature that reflects disease severity (by integrating MMP7, VCAM1, S100A12, ICAM1, and IL8) (28). Thus, we selected candidate markers with the aim to detect a characteristic signature of lung injury, fibrosis, and resolution in the bleomycin model. We found that sICAM1 was significantly increased at day 7 and remained increased as the injury was maintained. This expression was compartmentally regulated and detected in the blood, but not BALF. Compartmental regulation of ICAM1 is detected in IPF patients, where the levels of ICAM1 are higher in the peripheral blood than BALF (36).

The sICAM1 has been previously reported as a marker for epithelial injury in kidney disorders (39), since it is a target of proteinases that shed it from the cell membrane (11). Recently, in a cohort of lung-transplanted patients with primary graft dysfunction (34), sICAM1 was used as a predictor of mortality, which improved when sICAM1 was analyzed in combination with other markers (e.g. sICAM1 - PAI1 or sICAM1- sRAGE). Importantly, increased levels of sICAM1 in progressive injury have been reported in other models of lung injury (21). In fact, BALF levels of sICAM1 were associated with epithelial dynamics and transdifferentiation. Although our data does not show a significant increase in sICAM in the BALF of bleomycin-treated mice, we show that primary murine ATII cells from fibrotic mice secrete and/or shed higher levels of sICAM into the supernatant, demonstrating that lung ATII cells are an important source of sICAM during injury, fibrosis, and resolution thereof.

Interestingly, ICAM1 plays a critical role during lung injury and fibrosis in leucocyte kinetics. In arteries, ICAM1 does not increase during the initial injury and fibrotic phase of bleomycin-treated mice. Instead, in venules and capillaries, there is an increase in its expression, accompanied by an increase in leucocyte rolling, phenomenon inhibited by treatment with anti-ICAM1 monoclonal antibody (30). Furthermore, blockage of ICAM1 via monoclonal antibodies inhibits leucocyte recruitment, but does not decrease hydroxyproline content, or histopathological fibrosis, and therefore does not attenuate fibrosis (20). On the other hand, fibrotic ICAM1-/- mice exhibit decreased collagen content, when compared with littermate controls. Moreover, mice with double knockout for ICAM1 and L-selectin show a dramatic reduction in collagen deposition and fibrosis in response to bleomycin compared with littermate controls or single knockout mice (16). Taken together, these data suggest that ICAM1 determines the severity in lung fibrosis. Here, we show that not only endothelial cells, but also alveolar epithelial cells, express abundant amounts of ICAM1 during disease, which is actively secreted to their environment. As such, epithelial ICAM1, likely with help of other adhesion molecules, is a critical contributor to fibrosis via increased secretion/shedding of ICAM1 to the extracellular compartment.

Our data also shows that sICAM1 varies among individuals during the peak of fibrosis (day 14). Yet, this variation exhibited a strong correlation with compliance, reflecting that sICAM1 can monitor disease severity in mice. In humans, sICAM1 levels correlates with survival, even better when combined with other biomarkers. Shijubo and colleagues recently performed repetitive measures of ICAM1 in 4 IPF and one sarcoid patient. They found that in rapidly declining IPF patients (albeit with n=3), serum levels of ICAM1 gradually increased in repetitive visits, when disease worsened until death within a period of 3-12 months (35). Furthermore, Okuda and others (25) recently reported that in the early phase of acute exacerbations of IPF, ICAM1 is increased in IPF patients, and might serve as a predictive indicator for prognosis. Taking together, this data demonstrate that, similar to fibrotic mice, ICAM1 levels might predict disease severity, exacerbations, and mortality in IPF patients.

We initially measured sICAM1 in a multi-analyte bead-based assay with the Luminex platform. In order to corroborate our findings, we validated the upregulation of sICAM1 by ELISA, in which we observed a significant increase in sICAM1 at day 14. The differences in the concentrations of sICAM1 using the Luminex and ELISA assays likely results from multiple factors attributable to interassay variation, epitope specificity from manufacturer to manufacturer, dynamic range differences between fluorescence-based detection and absorbance-based assay quantification, all of which are currently debated parameters limiting the area of biomarker research (7).

In summary, our studies demonstrate that ICAM1 is expressed in the healthy lung epithelium. During injury and fibrosis, ICAM1 is shed and its plasma levels increase, which correlate well with lung function decline in experimental lung fibrosis. Plasma levels of sICAM1 measured at day 9 after the induction of fibrosis may predict worsening of lung function, and at the same time, higher levels of sICAM1 were associated with increased mortality. These studies indicate that sICAM1 could be considered as an indicator of ongoing lung injury and fibrosis and might help to monitor disease progression and therapeutic responses in preclinical models of fibrosis.

Acknowledgments

The authors thank Daniela Dietel, Constanze Heise, and Katharina Lippl for providing excellent technical assistance, and the Helmholtz Association for supporting this work.

FIGURE LEGENDS

***Figure 1*. Inflammatory cell recruitment and lung function during lung fibrosis.** C57BL/6 mice (aged 10–12 weeks, male) were treated with bleomycin or PBS and harvested at day 7, 14, 28 or 56 after treatment. PBS represents a pool of PBS-treated mice for 7, 14, 28, and 56 days. (A) Differential cell counts of inflammatory cells were assessed in broncho-alveolar lavage fluid. (B) Tissue stiffness was determined by lung function measurement of compliance and elastance. Data is presented in mean ± SD, for statistical analysis one-way ANOVA was used. For all experiments: *p<0.05, **p<0.01, ***p<0.001.

***Figure 2.* Semi-automatized quantification of lung fibrosis.** Hematoxylin-and-eosin staining of mouse lung sections from day 7, 14, 28 or 56 post treatment were scanned, analyzed, and quantified with Image J. PBS represents a pool of PBS-treated mice for 7, 14, 28, and 56 days. (A) Representative Masson trichrome stainings from PBS- or bleomycin-treated mice are depicted. (B) Threshold settings, 8-bit conversions, and area selections of H&E stainings are shown. (C) Quantification of alveolar space via Image J throughout the bleomycin time course is shown. Each dot represents the mean quantification of at least 3 whole-lobe sections per subject. Statistical differences (*p<0.05; **p<0.01; ***p<0.001) were determined by one-way ANOVA.

***Figure 3.* Correlation of lung function and histology over time in lung fibrosis.** Correlations between the % of alveolar space and lung compliance were determined using Pearson's correlation coefficient. (A) All-samples correlation including time point-matching PBS controls and 7, 14, 28, and 56 days treated mice. (B) Time point-specific correlations are shown.

***Figure 4.* The mRNA expression patterns of ECM markers in lung fibrosis.** The qRT-PCR analysis of expression levels of collagen-1a1 (*col1a1*), fibronectin (*fn1*), lysyl oxidase L2 (*loxl2*) and tenascin c (*tnc*), from PBS and bleomycin-treated mice harvested 7, 14, 28 and 56 days after treatment is shown. PBS

represents a pool of PBS-treated mice for 7, 14, 28, and 56 days. Data is presented in mean ± SD, as 1-ΔCT relative expression to control (GAPDH). Statistical differences (*p<0.05; **p<0.01; ***p<0.001) were determined by one-way ANOVA.

Figure 5. **Plasma and BALF biomarker profiling during lung injury and fibrosis.** MMP7 was measured by ELISA and MMP9, PAI1, E-selectin, VCAM1, and sICAM1 were measured by Luminex multiplex assay in plasma (A) and BALF (B) samples obtained from bleomycin- or PBS-treated mice over 7, 14, 28 and 56 days. In BALF measurement, VCAM1 and E-selectin were non-detectable, and "n" vary according to detectability. (C) sICAM1 ELISA using plasma samples from PBS- and bleomycin-treated mice. PBS represents a pool of PBS-treated mice for 7, 14, 28, and 56 days. Data is presented as mean ± SD. For statistical analysis one-way ANOVA was used. For all experiments: *p<0.05, **p<0.01, ***p<0.001.

Figure 6. **Correlation of lung function and plasma biomarkers in lung injury and fibrosis.** Correlation coefficients of lung compliance and plasma levels of selected candidates (MMP9, MMP7, PAI1, E-selectin, VCAM1, or sICAM1) were analyzed for subjects treated with bleomycin after day 7, 14, 28, 56 and respective PBS controls. Correlations between lung compliance and plasma signatures were determined using Pearson's correlation coefficient. Significance of the correlation analysis was set at p<0.05.

Figure 7. **Compartmentalization of ICAM1 levels during lung injury and fibrosis.** (A) Repetitive blood sampling every 3 days from day 0 to day 15 were obtained for PBS- (empty circle) and bleomycin-treated (red circle) mice, and plasma sICAM1 levels were analyzed. Statistical differences were determined by one-way ANOVA. (B) Whole lung homogenate protein levels of ICAM1 were assessed by Western blotting (n=3 blots were quantified by image densitometry). Relative protein levels are presented as ratio target protein to β-actin and normalized to PBS as 1. Statistical differences were determined by one-way ANOVA. (C) The pmATII cells were isolated from PBS- or bleomycin-treated mice (14 days) and

cultured for 5 days. Supernatants were collected and sICAM1 was measured by ELISA. Statistical differences were determined by t-test. (D) Immunofluorescence staining for ICAM1 (red), E-cadherin (green), and DAPI (blue) of PBS- (upper quadrants) and bleomycin-treated (14 days) mice (lower quadrants). Gray squares show lower magnification of zoomed areas (right), the scale bar represents 50μm in non-zoom pictures (left), and 20μm in zoomed pictures (right). For all experiments significance was set: *$p<0.05$, **$p<0.01$, ***$p<0.001$.

REFERENCES

1. **Ask K, Labiris R, Farkas L, Moeller A, Froese A, Farncombe T, McClelland GB, Inman M, Gauldie J, and Kolb MR**. Comparison between conventional and "clinical" assessment of experimental lung fibrosis. *J Transl Med* 6: 16, 2008.
2. **B BM, Lawson WE, Oury TD, Sisson TH, Raghavendran K, and Hogaboam CM**. Animal models of fibrotic lung disease. *Am J Respir Cell Mol Biol* 49: 167-179, 2013.
3. **Barkauskas CE, and Noble PW**. Cellular mechanisms of tissue fibrosis. 7. New insights into the cellular mechanisms of pulmonary fibrosis. *Am J Physiol Cell Physiol* 306: C987-996, 2014.
4. **Bauer Y, Tedrow J, de Bernard S, Birker-Robaczewska M, Gibson KF, Guardela BJ, Hess P, Klenk A, Lindell KO, Poirey S, Renault B, Rey M, Weber E, Nayler O, and Kaminski N**. A novel genomic signature with translational significance for human idiopathic pulmonary fibrosis. *Am J Respir Cell Mol Biol* 52: 217-231, 2015.
5. **Behr J**. Evidence-based treatment strategies in idiopathic pulmonary fibrosis. *Eur Respir Rev* 22: 163-168, 2013.
6. **Bonniaud P, Margetts PJ, Kolb M, Haberberger T, Kelly M, Robertson J, and Gauldie J**. Adenoviral gene transfer of connective tissue growth factor in the lung induces transient fibrosis. *American journal of respiratory and critical care medicine* 168: 770-778, 2003.
7. **Breen EC, Reynolds SM, Cox C, Jacobson LP, Magpantay L, Mulder CB, Dibben O, Margolick JB, Bream JH, Sambrano E, Martinez-Maza O, Sinclair E, Borrow P, Landay AL, Rinaldo CR, and Norris PJ**. Multisite comparison of high-sensitivity multiplex cytokine assays. *Clinical and vaccine immunology : CVI* 18: 1229-1242, 2011.
8. **Casoni GL, Tomassetti S, Cavazza A, Colby TV, Dubini A, Ryu JH, Carretta E, Tantalocco P, Piciucchi S, Ravaglia C, Gurioli C, Romagnoli M, Gurioli C, Chilosi M, and Poletti V**. Transbronchial lung cryobiopsy in the diagnosis of fibrotic interstitial lung diseases. *PLoS One* 9: e86716, 2014.
9. **Dancey C, and Reidy J**. *Statistics without Maths for Psychology: using SPSS for Windows*. London: Prentice Hall, 2004.
10. **du Bois RM**. Strategies for treating idiopathic pulmonary fibrosis. *Nat Rev Drug Discov* 9: 129-140, 2010.
11. **Essick E, Sithu S, Dean W, and D'Souza S**. Pervanadate-induced shedding of the intercellular adhesion molecule (ICAM)-1 ectodomain is mediated by membrane type-1 matrix metalloproteinase (MT1-MMP). *Mol Cell Biochem* 314: 151-159, 2008.
12. **Fernandez IE, and Eickelberg O**. The impact of TGF-beta on lung fibrosis: from targeting to biomarkers. *Proc Am Thorac Soc* 9: 111-116, 2012.
13. **Fernandez IE, and Eickelberg O**. New cellular and molecular mechanisms of lung injury and fibrosis in idiopathic pulmonary fibrosis. *Lancet* 380: 680-688, 2012.
14. **Flaherty KR, and Khanna D**. Idiopathic or connective tissue disease-associated interstitial lung disease: a case of HRCT mimicry. *Thorax* 69: 205-206, 2014.
15. **Hadi AM, Mouchaers KT, Schalij I, Grunberg K, Meijer GA, Vonk-Noordegraaf A, van der Laarse WJ, and Belien JA**. Rapid quantification of myocardial fibrosis: a new macro-based automated analysis. *Cell Oncol (Dordr)* 34: 343-354, 2011.
16. **Hamaguchi Y, Nishizawa Y, Yasui M, Hasegawa M, Kaburagi Y, Komura K, Nagaoka T, Saito E, Shimada Y, Takehara K, Kadono T, Steeber DA, Tedder TF, and Sato S**. Intercellular adhesion molecule-1 and L-selectin regulate bleomycin-induced lung fibrosis. *Am J Pathol* 161: 1607-1618, 2002.
17. **John G, Kohse K, Orasche J, Reda A, Schnelle-Kreis J, Zimmermann R, Schmid O, Eickelberg O, and Yildirim AO**. The composition of cigarette smoke determines inflammatory cell recruitment to the lung in COPD mouse models. *Clin Sci (Lond)* 126: 207-221, 2014.

18. **King TE, Jr., Bradford WZ, Castro-Bernardini S, Fagan EA, Glaspole I, Glassberg MK, Gorina E, Hopkins PM, Kardatzke D, Lancaster L, Lederer DJ, Nathan SD, Pereira CA, Sahn SA, Sussman R, Swigris JJ, Noble PW, and Group AS**. A phase 3 trial of pirfenidone in patients with idiopathic pulmonary fibrosis. *N Engl J Med* 370: 2083-2092, 2014.
19. **Ley B, Bradford WZ, Vittinghoff E, Weycker D, du Bois RM, and Collard HR**. Predictors of Mortality Poorly Predict Common Measures of Disease Progression in Idiopathic Pulmonary Fibrosis. *American journal of respiratory and critical care medicine* 2016.
20. **Matsuse T, Teramoto S, Katayama H, Sudo E, Ekimoto H, Mitsuhashi H, Uejima Y, Fukuchi Y, and Ouchi Y**. ICAM-1 mediates lung leukocyte recruitment but not pulmonary fibrosis in a murine model of bleomycin-induced lung injury. *Eur Respir J* 13: 71-77, 1999.
21. **Mendez MP, Morris SB, Wilcoxen S, Greeson E, Moore B, and Paine R, 3rd**. Shedding of soluble ICAM-1 into the alveolar space in murine models of acute lung injury. *Am J Physiol Lung Cell Mol Physiol* 290: L962-970, 2006.
22. **Mercer PF, Abbott-Banner K, Adcock IM, and Knowles RG**. Translational models of lung disease. *Clin Sci (Lond)* 128: 235-256, 2015.
23. **Mouratis MA, and Aidinis V**. Modeling pulmonary fibrosis with bleomycin. *Curr Opin Pulm Med* 17: 355-361, 2011.
24. **Mutze K, Vierkotten S, Milosevic J, Eickelberg O, and Konigshoff M**. Enolase 1 (ENO1) and protein disulfide-isomerase associated 3 (PDIA3) regulate Wnt/beta-catenin-driven trans-differentiation of murine alveolar epithelial cells. *Dis Model Mech* 8: 877-890, 2015.
25. **Okuda R, Matsushima H, Aoshiba K, Oba T, Kawabe R, Honda K, and Amano M**. Soluble intercellular adhesion molecule-1 for stable and acute phases of idiopathic pulmonary fibrosis. *Springerplus* 4: 657, 2015.
26. **Peng R, Sridhar S, Tyagi G, Phillips JE, Garrido R, Harris P, Burns L, Renteria L, Woods J, Chen L, Allard J, Ravindran P, Bitter H, Liang Z, Hogaboam CM, Kitson C, Budd DC, Fine JS, Bauer CM, and Stevenson CS**. Bleomycin induces molecular changes directly relevant to idiopathic pulmonary fibrosis: a model for "active" disease. *PLoS One* 8: e59348, 2013.
27. **Raghu G, Collard HR, Egan JJ, Martinez FJ, Behr J, Brown KK, Colby TV, Cordier JF, Flaherty KR, Lasky JA, Lynch DA, Ryu JH, Swigris JJ, Wells AU, Ancochea J, Bouros D, Carvalho C, Costabel U, Ebina M, Hansell DM, Johkoh T, Kim DS, King TE, Jr., Kondoh Y, Myers J, Muller NL, Nicholson AG, Richeldi L, Selman M, Dudden RF, Griss BS, Protzko SL, Schunemann HJ, and Fibrosis AEJACoIP**. An official ATS/ERS/JRS/ALAT statement: idiopathic pulmonary fibrosis: evidence-based guidelines for diagnosis and management. *American journal of respiratory and critical care medicine* 183: 788-824, 2011.
28. **Richards TJ, Kaminski N, Baribaud F, Flavin S, Brodmerkel C, Horowitz D, Li K, Choi J, Vuga LJ, Lindell KO, Klesen M, Zhang Y, and Gibson KF**. Peripheral blood proteins predict mortality in idiopathic pulmonary fibrosis. *American journal of respiratory and critical care medicine* 185: 67-76, 2012.
29. **Richeldi L, du Bois RM, Raghu G, Azuma A, Brown KK, Costabel U, Cottin V, Flaherty KR, Hansell DM, Inoue Y, Kim DS, Kolb M, Nicholson AG, Noble PW, Selman M, Taniguchi H, Brun M, Le Maulf F, Girard M, Stowasser S, Schlenker-Herceg R, Disse B, Collard HR, and Investigators IT**. Efficacy and safety of nintedanib in idiopathic pulmonary fibrosis. *N Engl J Med* 370: 2071-2082, 2014.
30. **Sato N, Suzuki Y, Nishio K, Suzuki K, Naoki K, Takeshita K, Kudo H, Miyao N, Tsumura H, Serizawa H, Suematsu M, and Yamaguchi K**. Roles of ICAM-1 for abnormal leukocyte recruitment in the microcirculation of bleomycin-induced fibrotic lung injury. *American journal of respiratory and critical care medicine* 161: 1681-1688, 2000.
31. **Schiller HB, Fernandez IE, Burgstaller G, Schaab C, Scheltema RA, Schwarzmayr T, Strom TM, Eickelberg O, and Mann M**. Time- and compartment-resolved proteome profiling of the extracellular niche in lung injury and repair. *Mol Syst Biol* 11: 819, 2015.

32. **Schmidt SL, Tayob N, Han MK, Zappala C, Kervitsky D, Murray S, Wells AU, Brown KK, Martinez FJ, and Flaherty KR**. Predicting pulmonary fibrosis disease course from past trends in pulmonary function. *Chest* 145: 579-585, 2014.
33. **Scotton CJ, Hayes B, Alexander R, Datta A, Forty EJ, Mercer PF, Blanchard A, and Chambers RC**. Ex vivo micro-computed tomography analysis of bleomycin-induced lung fibrosis for preclinical drug evaluation. *Eur Respir J* 42: 1633-1645, 2013.
34. **Shah RJ, Bellamy SL, Localio AR, Wickersham N, Diamond JM, Weinacker A, Lama VN, Bhorade S, Belperio JA, Crespo M, Demissie E, Kawut SM, Wille KM, Lederer DJ, Lee JC, Palmer SM, Orens J, Reynolds J, Shah A, Wilkes DS, Ware LB, and Christie JD**. A panel of lung injury biomarkers enhances the definition of primary graft dysfunction (PGD) after lung transplantation. *J Heart Lung Transplant* 31: 942-949, 2012.
35. **Shijubo N, Imai K, Aoki S, Hirasawa M, Sugawara H, Koba H, Tsujisaki M, Sugiyama T, Hinoda Y, Yachi A, and et al.** Circulating intercellular adhesion molecule-1 (ICAM-1) antigen in sera of patients with idiopathic pulmonary fibrosis. *Clin Exp Immunol* 89: 58-62, 1992.
36. **Shijubo N, Imai K, Shigehara K, Honda Y, Koba H, Tsujisaki M, Hinoda Y, Yachi A, Ohmichi M, Hiraga Y, and et al.** Soluble intercellular adhesion molecule-1 (ICAM-1) in sera and bronchoalveolar lavage fluid of patients with idiopathic pulmonary fibrosis and pulmonary sarcoidosis. *Clin Exp Immunol* 95: 156-161, 1994.
37. **Staab-Weijnitz CA, Fernandez IE, Knuppel L, Maul J, Heinzelmann K, Juan-Guardela BM, Hennen E, Preissler G, Winter H, Neurohr C, Hatz R, Lindner M, Behr J, Kaminski N, and Eickelberg O**. FK506-Binding Protein 10, a Potential Novel Drug Target for Idiopathic Pulmonary Fibrosis. *American journal of respiratory and critical care medicine* 192: 455-467, 2015.
38. **Strand MJ, Sprunger D, Cosgrove GP, Fernandez-Perez ER, Frankel SK, Huie TJ, Olson AL, Solomon J, Brown KK, and Swigris JJ**. Pulmonary function and survival in idiopathic vs secondary usual interstitial pneumonia. *Chest* 146: 775-785, 2014.
39. **Therrien FJ, Agharazii M, Lebel M, and Lariviere R**. Neutralization of tumor necrosis factor-alpha reduces renal fibrosis and hypertension in rats with renal failure. *Am J Nephrol* 36: 151-161, 2012.
40. **Walsh SL, Sverzellati N, Devaraj A, Keir GJ, Wells AU, and Hansell DM**. Connective tissue disease related fibrotic lung disease: high resolution computed tomographic and pulmonary function indices as prognostic determinants. *Thorax* 69: 216-222, 2014.
41. **Wells AU, Desai SR, Rubens MB, Goh NS, Cramer D, Nicholson AG, Colby TV, du Bois RM, and Hansell DM**. Idiopathic pulmonary fibrosis: a composite physiologic index derived from disease extent observed by computed tomography. *American journal of respiratory and critical care medicine* 167: 962-969, 2003.
42. **Wynn TA, and Ramalingam TR**. Mechanisms of fibrosis: therapeutic translation for fibrotic disease. *Nat Med* 18: 1028-1040, 2012.

Fig.1

A

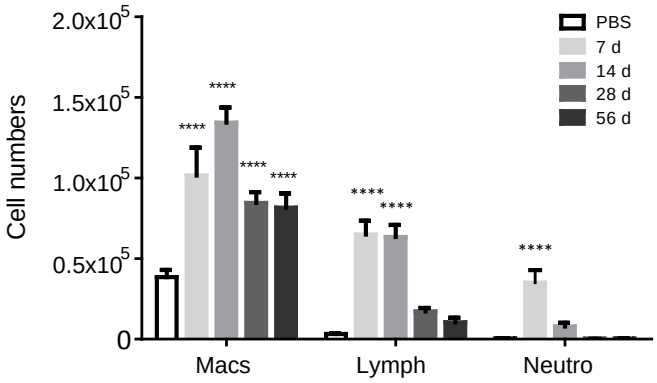
Cell numbers
2.0x10^5
1.5x10^5
1.0x10^5
0.5x10^5
0
PBS
7 d
14 d
28 d
56 d
****
Macs
Lymph
Neutro

B

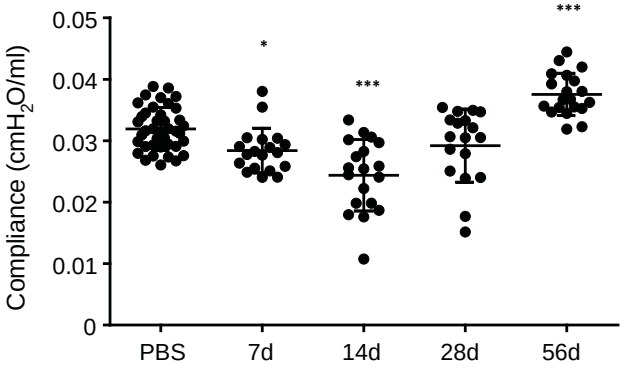
Compliance (cmH2O/ml)
0.05
0.04
0.03
0.02
0.01
0
*
***
PBS
7d
14d
28d
56d

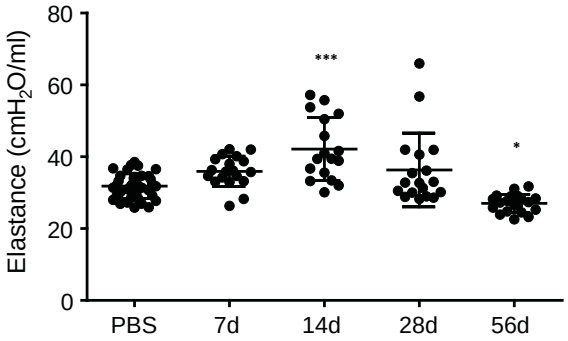
Elastance (cmH2O/ml)
80
60
40
20
0
***
*
PBS
7d
14d
28d
56d

Fig.2

A

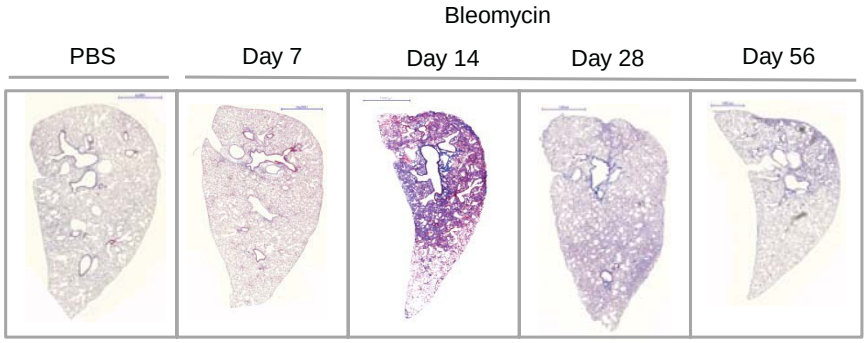
Bleomycin
PBS
Day 7
Day 14
Day 28
Day 56

B

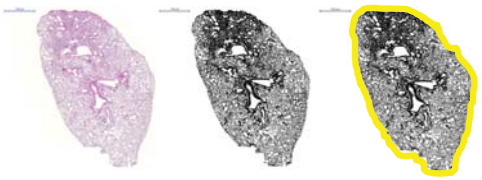

C

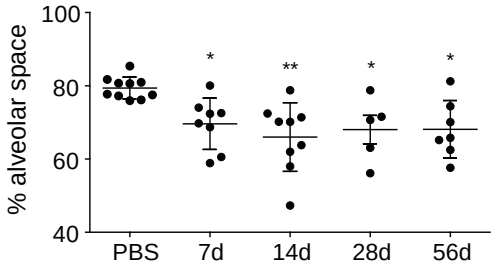
% alveolar space
100
80
60
40
*
**
*
*
PBS
7d
14d
28d
56d

Fig.3

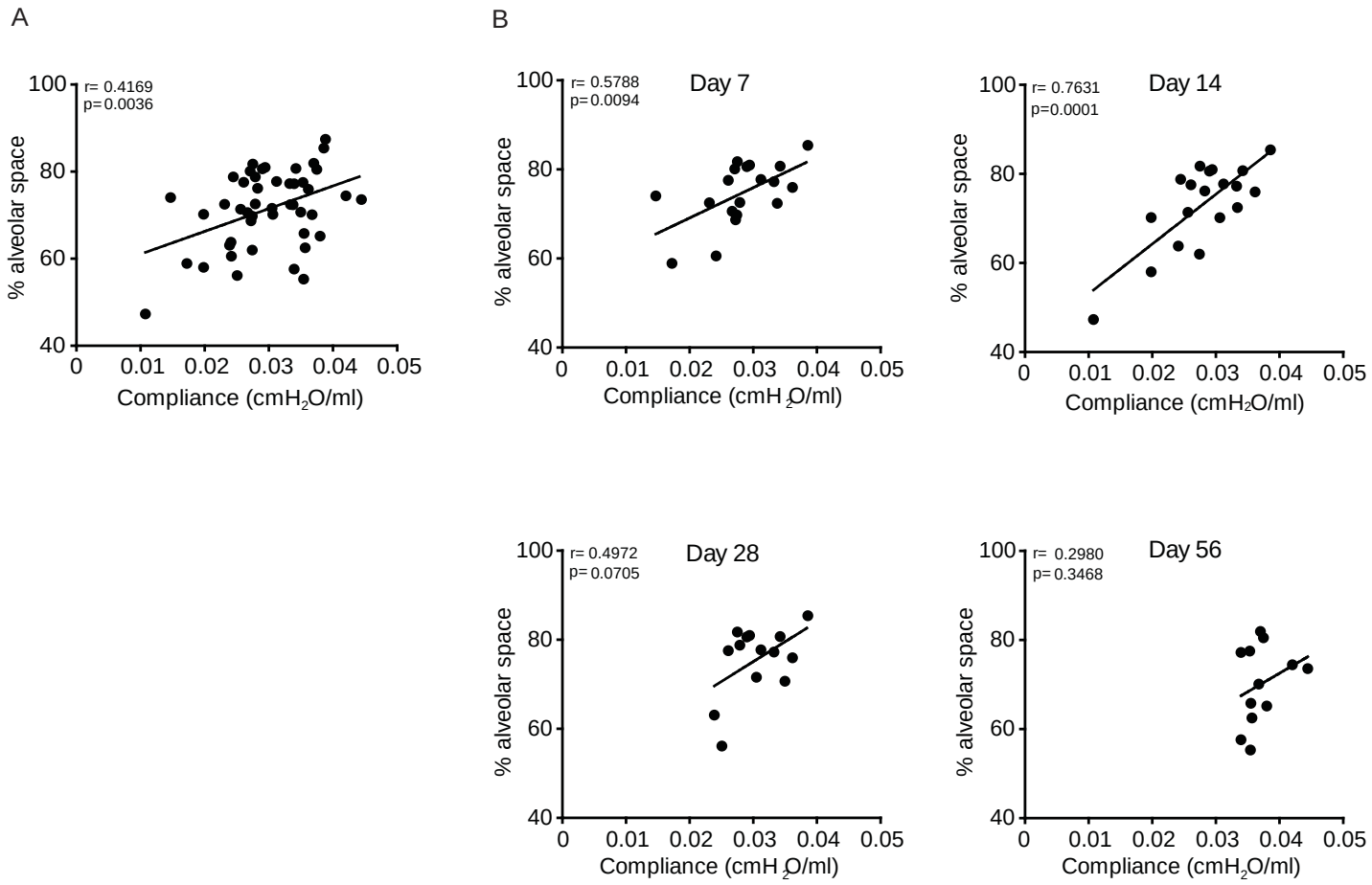
A
B
r= 0.4169
p=0.0036
% alveolar space
Compliance (cmH2O/ml)
Day 7
r= 0.5788
p=0.0094
Day 14
r= 0.7631
p=0.0001
Day 28
r= 0.4972
p= 0.0705
Day 56
r= 0.2980
p= 0.3468

Fig.4

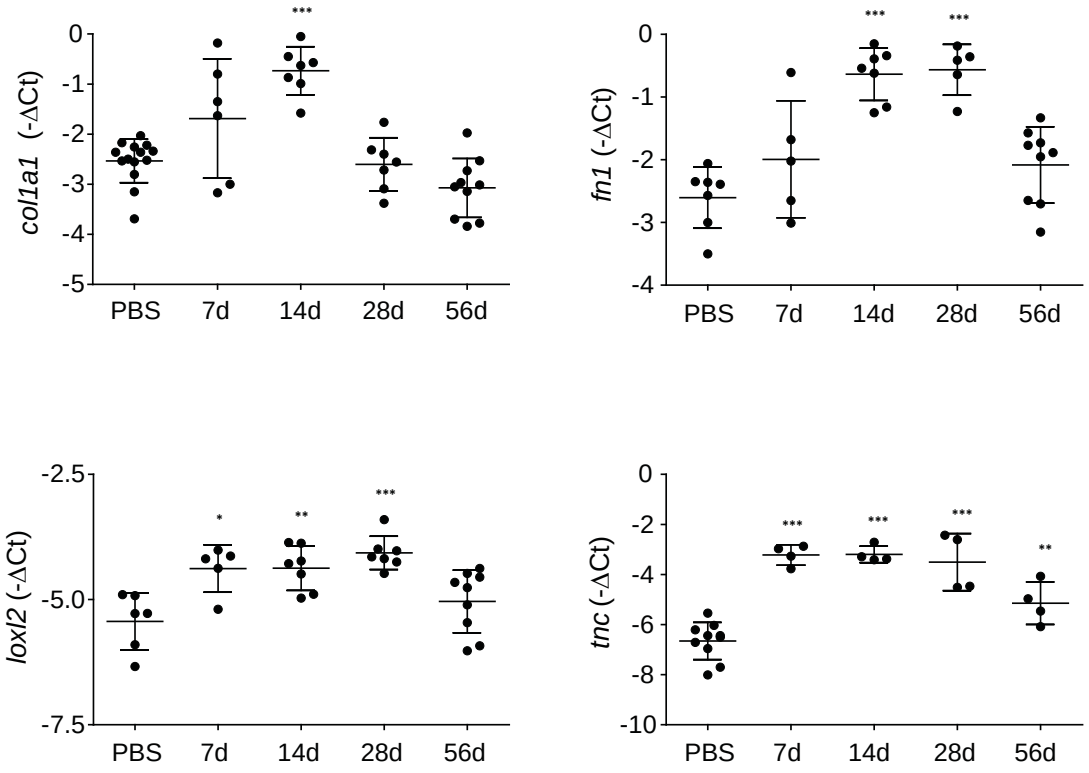
col1a1 (-ΔCt)
0
-1
-2
-3
-4
-5
***
PBS
7d
14d
28d
56d
fn1 (-ΔCt)
0
-1
-2
-3
-4
***
***
PBS
7d
14d
28d
56d
loxl2 (-ΔCt)
-2.5
-5.0
-7.5
*
**
***
PBS
7d
14d
28d
56d
tnc (-ΔCt)
0
-2
-4
-6
-8
-10
***
***
***
**
PBS
7d
14d
28d
56d

Fig.5

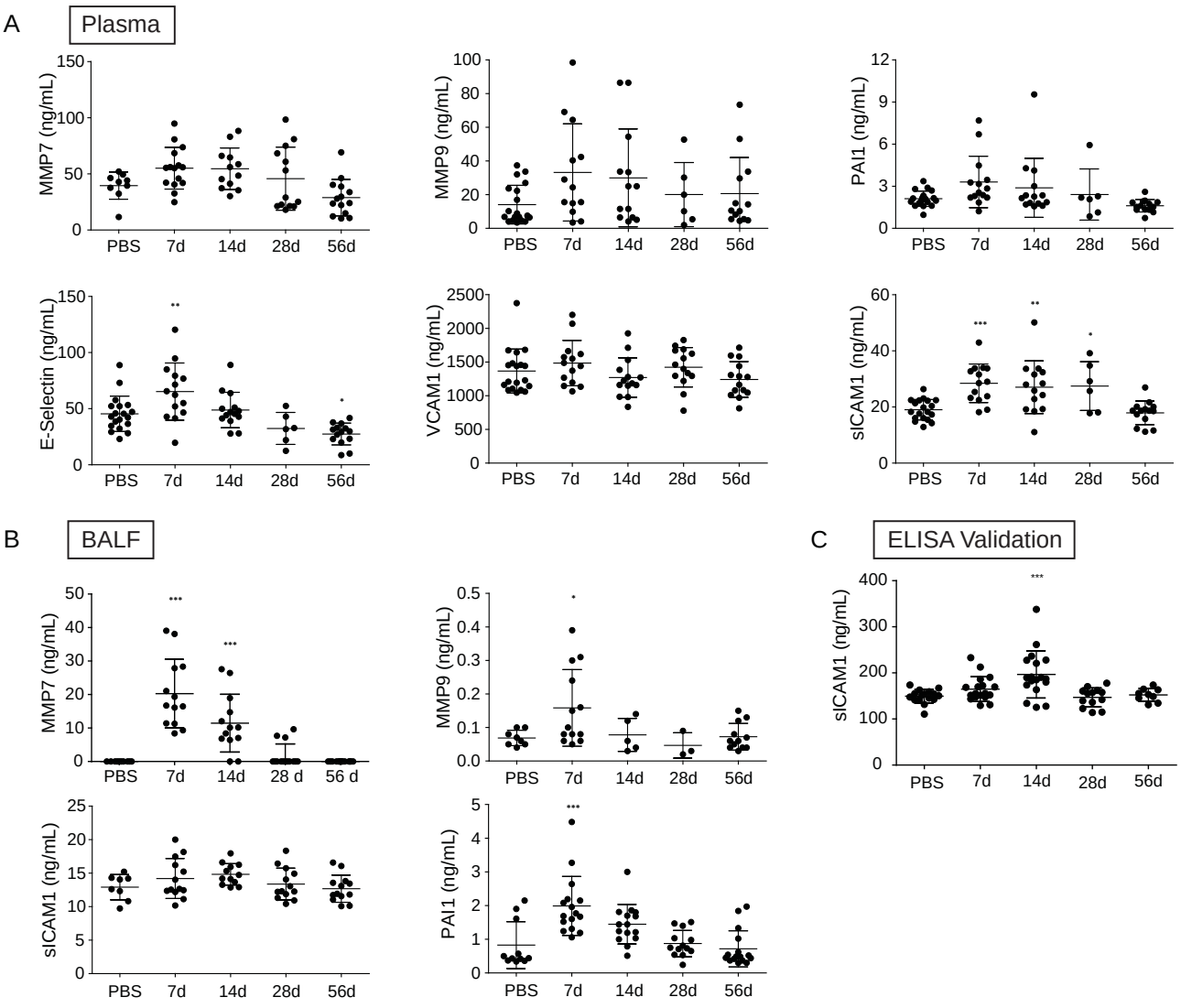
A
Plasma
MMP7 (ng/mL)
MMP9 (ng/mL)
PAI1 (ng/mL)
E-Selectin (ng/mL)
VCAM1 (ng/mL)
sICAM1 (ng/mL)
PBS
7d
14d
28d
56d
B
BALF
MMP7 (ng/mL)
MMP9 (ng/mL)
sICAM1 (ng/mL)
PAI1 (ng/mL)
PBS
7d
14d
28 d
56 d
C
ELISA Validation
sICAM1 (ng/mL)

Fig.6

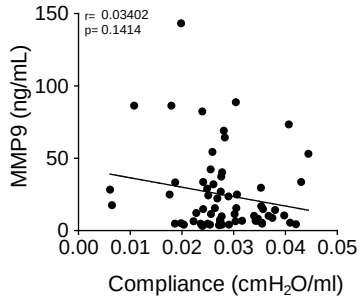
r= 0.03402
p= 0.1414
MMP9 (ng/mL)
150
100
50
0
0.00 0.01 0.02 0.03 0.04 0.05
Compliance (cmH2O/ml)

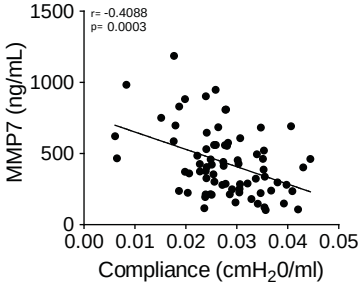
r= -0.4088
p= 0.0003
MMP7 (ng/mL)
1500
1000
500
0
0.00 0.01 0.02 0.03 0.04 0.05
Compliance (cmH20/ml)

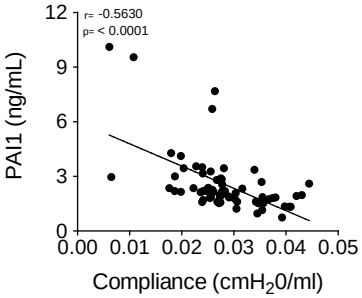
r= -0.5630
p= < 0.0001
PAI1 (ng/mL)
12
9
6
3
0
0.00 0.01 0.02 0.03 0.04 0.05
Compliance (cmH20/ml)

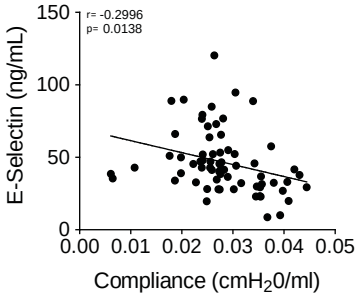
r= -0.2996
p= 0.0138
E-Selectin (ng/mL)
150
100
50
0
0.00 0.01 0.02 0.03 0.04 0.05
Compliance (cmH20/ml)

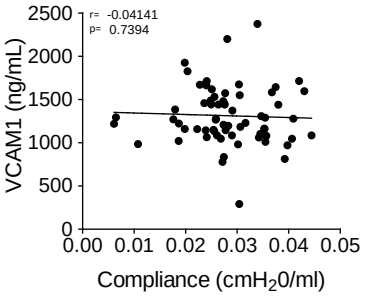
r= -0.04141
p= 0.7394
VCAM1 (ng/mL)
2500
2000
1500
1000
500
0
0.00 0.01 0.02 0.03 0.04 0.05
Compliance (cmH20/ml)

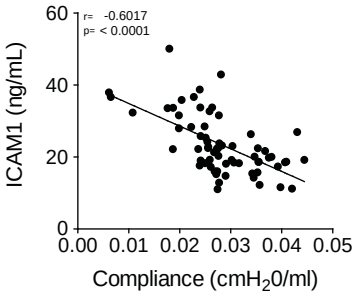
r= -0.6017
p= < 0.0001
ICAM1 (ng/mL)
60
40
20
0
0.00 0.01 0.02 0.03 0.04 0.05
Compliance (cmH20/ml)

Fig.7

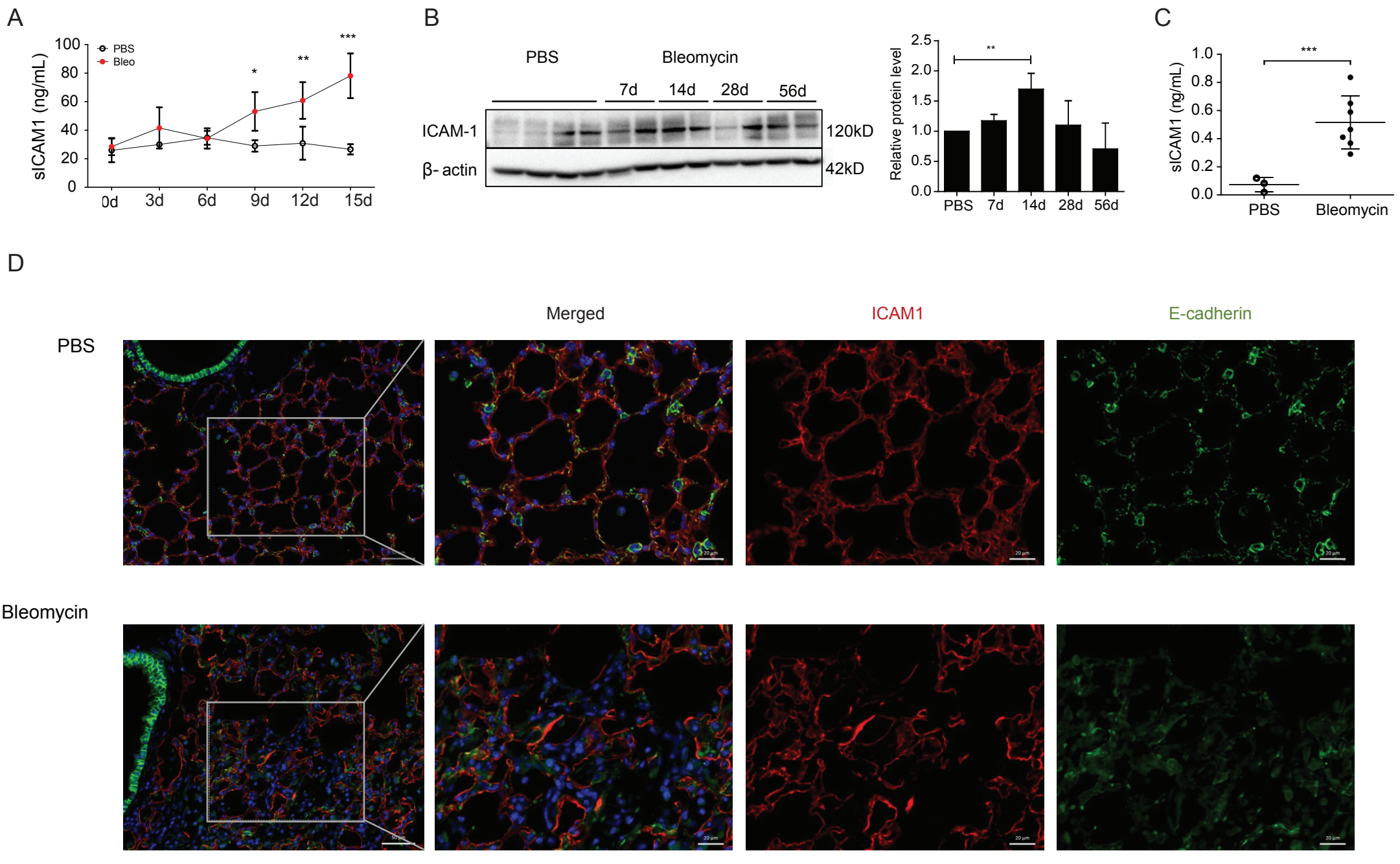
A
sICAM1 (ng/mL)
PBS
Bleo
0d
3d
6d
9d
12d
15d
B
PBS
Bleomycin
7d
14d
28d
56d
ICAM-1
β- actin
120kD
42kD
Relative protein level
C
sICAM1 (ng/mL)
PBS
Bleomycin
D
Merged
ICAM1
E-cadherin
PBS
Bleomycin